




# Magnesium Green for fluorometric measurement of ATP production does not interfere with mitochondrial respiration

 Luiza HD Cardoso\*,  Carolina Doerrier,  Erich Gnaiger

Oroboros Instruments, Innsbruck, Austria

\*Corresponding author: luiza.cardoso@orooboros.at

## Abstract

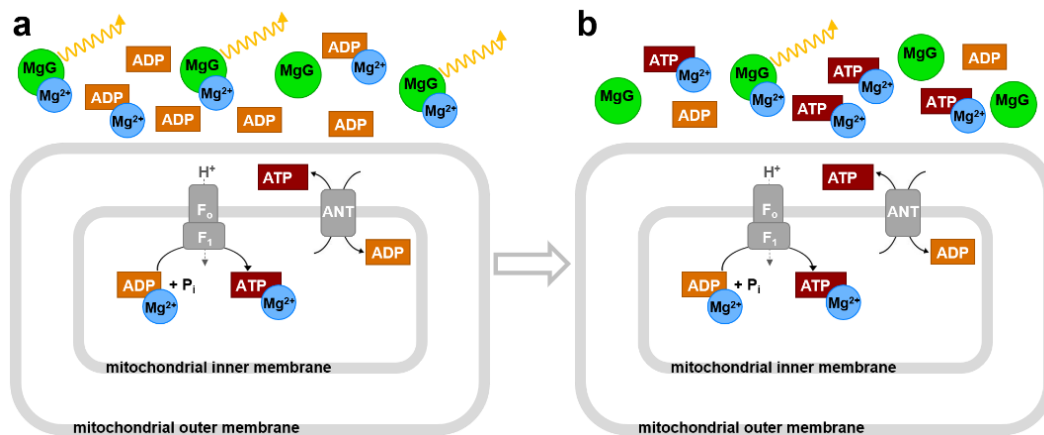
For the advanced study of mitochondrial function, high-resolution respirometry is extended by fluorometric measurement of ATP production using the fluorophore Magnesium Green™ (MgG). A common problem with several fluorescent dyes is the inhibition of mitochondrial respiration. In the present study, a coupling control protocol was applied in combination with MgG to measure ATP production simultaneously with respiration for calculation of  $P_{\text{O}_2}/\text{O}_2$  ratios. MgG at 1.1  $\mu\text{M}$  did not affect respiration through the NADH-linked and succinate-linked pathways. Respiration was not inhibited in any of the coupling control states, hence coupling control efficiencies were not affected by MgG.

*Keywords* – ATP; ATP production; high-resolution respirometry; Magnesium Green; mitochondria; oxidative phosphorylation; fluorometry; FluoRespirometry

## 1. Introduction

Mitochondrial ATP production can be analyzed with a fluorometric technique using Magnesium Green™ (MgG) as a fluorescent probe, as described by Chinopoulos et al (2009). Application of the  $\text{Mg}^{2+}$ -sensitive fluorophore as an indicator of ATP production relies on the fact that ADP and ATP have different affinities for  $\text{Mg}^{2+}$  (Gnaiger, Wyss 1994; Leyssens et al 1996; Budinger et al 1998). ADP is phosphorylated to ATP in the mitochondrial matrix. In the phosphorylation system ADP/ATP and inorganic phosphate  $\text{P}_i$  are exchanged stoichiometrically by the adenine nucleotide translocase ANT and the phosphate carrier PiC. Under experimental conditions when ADP decreases while ATP increases in the extramitochondrial milieu, the  $\text{Mg}^{2+}$  concentration declines due to the higher affinity for  $\text{Mg}^{2+}$  of ATP than ADP (Figure 1). Therefore, the fluorometric assay with the membrane-impermeant MgG provides a quantitative approach to analyze mitochondrial ATP production. This method was developed further to measure concomitantly mitochondrial ATP production and  $\text{O}_2$  consumption in the Oroboros O2k-FluoRespirometer which is an experimental system complete for high-resolution respirometry including fluorometry (Chinopoulos et al 2014).

41 Fluorescent dyes are widely used to assess various parameters relevant in  
 42 mitochondrial physiology. Safranin, rhodamine and its derivatives, such as TMRM, are  
 43 frequently employed as reporters of the mitochondrial membrane potential  $\Delta\Psi_p+$ .  
 44 However, all  $\Delta\Psi_p+$  dyes have been shown to affect mitochondrial respiration (Scaduto,  
 45 Grotjohann 1999). Like TPP<sup>+</sup>, safranin mainly affects the NADH (N)-linked pathway, the  
 46 phosphorylation system, and to a smaller extent the succinate (S)-linked pathway  
 47 (Krumshchnabel et al 2014). The effect of  $\Delta\Psi_p+$  fluorescent probes can be explained since  
 48 they accumulate in the mitochondrial matrix and thus possibly affect mitochondrial  
 49 function.  
 50



51 **Figure 1. Concept of the MgG assay according to Chinopoulos et al (2014).** MgG  
 52 fluoresces when bound to Mg<sup>2+</sup>. ADP and ATP compete for Mg<sup>2+</sup> binding with different  
 53 affinities; ATP has a higher affinity for Mg<sup>2+</sup> compared to ADP. **(a)** Initial experimental  
 54 conditions, when ADP is added, binding some Mg<sup>2+</sup>, and high MgG fluorescence drops  
 55 slightly. **(b)** As the experiment proceeds, ADP is phosphorylated to ATP, which is  
 56 exchanged for ADP by the adenine nucleotide translocase ANT. With increase in ATP in  
 57 the extramitochondrial medium, more Mg<sup>2+</sup> is bound to ATP, and MgG fluorescence  
 58 decreases.  
 59

60 It is important to note that another dye frequently used in mitochondrial physiology  
 61 studies, Amplex UltraRed, employed to analyze H<sub>2</sub>O<sub>2</sub> production, was shown to affect  
 62 mitochondrial respiration even though the mitochondrial membranes are not permeable  
 63 to this fluorophore (Makrecka-Kuka et al 2015). Therefore, it is important to analyze  
 64 whether MgG affects mitochondrial respiration, despite the fact that mitochondrial  
 65 membranes are not permeable to this fluorophore.  
 66

67 In the present technical communication, we report the effect of MgG on  
 68 mitochondrial respiration, which is the gold standard to evaluate mitochondrial function.  
 69 This provides an important contribution towards further development of this method to  
 70 analyze P<sub>o</sub>/O<sub>2</sub> ratios in different mitochondrial preparations. The use of a coupling  
 71 control protocol assessing O<sub>2</sub> consumption and MgG fluorescence allows for the  
 72 evaluation of mitochondrial respiration and ATP production using NADH- and succinate-  
 73 linked substrates in LEAK, OXPHOS- and ET-state, making it possible to obtain flux control  
 74 efficiencies.

## 2. Materials and methods

### 2.1. Reagents

Magnesium Green was purchased from Invitrogen/Thermo Fisher Scientific (cat. N° M3733). Antimycin A (cat. N° A8674), ATP (cat. N° A2383), CCCP (cat. N° C2759), malate (cat. N° M1000), MgCl<sub>2</sub> 1 M (cat. N° M1028), oligomycin (cat. N° O4876), pyruvate (cat. N° P2256), rotenone (cat. N° R8875), SF 6847 (cat. N° T182), and succinate (cat. N° S2378) were obtained from Sigma Aldrich. ADP was acquired from Millipore (cat. N° 117105), and carboxyatractyloside from Calbiochem (cat. N° 216201).

ADP and ATP were diluted in deionized H<sub>2</sub>O without addition of Mg<sup>2+</sup> salts, pH was adjusted to 6.9 with KOH. Magnesium Green, malate, succinate, carboxyatractyloside and MgCl<sub>2</sub> were diluted in deionized H<sub>2</sub>O whereas antimycin A, CCCP, oligomycin, rotenone and SF 6847 were diluted in ethanol p.a. All solutions were aliquoted and stored at -20 °C, except pyruvate, which was diluted in deionized H<sub>2</sub>O fresh on the day of each experiment.

### 2.2. Animals

Wild-type C57BL/6N adult mice (*N*=3 per experimental group) were housed in the animal facility of the Medical University of Innsbruck (maximum 5 mice per cage) and, maintained at 22 °C with a controlled 12 h light/dark cycle. Mice were fed *ad libitum* with free access to water. All procedures were conducted according to the Austrian Animal Experimentation Act in compliance with the European convention for the protection of vertebrate animals used for experimental and other scientific purposes (Tierversuchsgesetz 2012; Directive 2010/63/EU; BMWFM-66.011/0128-WF/V/3b/2016).

### 2.3. Cardiac mitochondrial isolation and protein concentration determination

Following cervical dislocation, the hearts were immediately excised and transferred into ice-cold biopsy preservation solution (BIOPS: 10 mM Ca<sup>2+</sup>-EGTA - 0.1 μM free Ca<sup>2+</sup>, 20 mM imidazole, 20 mM taurine, 50 mM K<sup>+</sup>-MES, 0.5 mM dithiothreitol, 6.56 mM MgCl<sub>2</sub>, 5.77 mM ATP, 15 mM phosphocreatine, pH 7.1 adjusted with KOH) for short period of time (1–2 h; Fontana-Ayoub et al 2016). All procedures were performed on ice (Gnaiger et al 2000a). Mouse heart mitochondria were isolated following the protocol described by Fontana-Ayoub and Krumschnabel (2015). The heart (~ 80–120 mg) was washed to remove blood clots and minced with 1 mL of BIOPS. The tissue was homogenized with 2 mL isolation buffer (IB1: 0.5 M mannitol; 0.5 M sucrose; 0.1 M EGTA; pH 7.4 adjusted with Tris; 2.5 mg/mL BSA and 0.5 mg/mL subtilisin, the latter two added freshly on the day of use) on a 10 mL glass-Teflon Potter Elvehjem homogenizer, 6–8 × with about 1000 rpm mechanical rotation. 3 mL of IB1 was added to the homogenate which was centrifuged at 800 *g* for 10 min at 4 °C. The supernatant was centrifuged again, at 10 000 *g* for 10 min at 4 °C. The pellet was resuspended carefully using a 1 mL pipette in 0.5 mL IB2 (IB1 without subtilisin). After addition of 2 mL IB2, the homogenate was centrifuged again at 10 000 *g* for 10 min at 4 °C. The pellet was resuspended in 200 μL of IB3 (IB1 without BSA and subtilisin) and kept on ice until use on the same day within 2 h.

122 Protein concentration was used for calculation of mass specific O<sub>2</sub> flux, determined  
123 using the kit DC Protein Assay (Bio-Rad, Hercules, CA, US). Absorbance was measured at  
124 620 nm with a Tecan Infinite TM F200 spectrophotometer (Tecan, Männedorf,  
125 Switzerland), using BSA at different concentrations as standards (Lowry et al 1951).  
126

#### 127 *2.4. High-resolution respirometry*

128

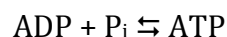
129 Oxygen consumption and ATP production measurements were performed  
130 simultaneously at 37 °C in the O2k-FluoRespirometer (O2k, Oroboros Instruments,  
131 Innsbruck, Austria). The O2k includes two Duran® glass chambers with stirring (750  
132 rpm) and controlled temperature for closed-chamber respirometry using polarographic  
133 oxygen sensors (POS). Smart Fluo-Sensors Blue were used, with excitation LED 465 nm  
134 and filters for the LED and photodiode selected for Magnesium Green™). Specific  
135 amperometric emission and detection settings – fluorescence light intensity of 500 and  
136 gain 100 – were applied with the software DatLab 7.4 (Oroboros Instruments, Innsbruck,  
137 Austria) with continuous data recording set at 2 s time intervals. Standardized  
138 calibrations and instrumental O<sub>2</sub> background tests were performed (Doerrier et al 2018).  
139 The time-derivative of the O<sub>2</sub> concentration is calculated real-time by DatLab, providing  
140 traces of O<sub>2</sub> flux corrected for the O<sub>2</sub> instrumental background (Gnaiger 2001).  
141

142 Experiments were run with cardiac isolated mitochondria at protein concentrations  
143 in the range of 0.026–0.049 mg/mL in modified mitochondrial respiration medium  
144 MiR05-MgG (MgCl<sub>2</sub> 1 mM instead of 3 mM in MiR05, EGTA 0,5 mM, KH<sub>2</sub>PO<sub>4</sub> 10 mM, Hepes  
145 20 mM, lactobionic acid 60 mM, D-sucrose 110 mM, taurine 20 mM, BSA 1 g/L, pH  
146 adjusted with KOH to 7.1). This modification of MiR05 (Gnaiger et al 2000a) was  
147 optimized for measurement of ATP production with MgG.  
148

#### 149 *2.5. ATP production measurement with MgG*

150

151 MgG (Magnesium Green™, pentapotassium salt, cell impermeant) does not  
152 permeate biological membranes. Therefore, the plasma membrane barrier function must  
153 be removed, as achieved in mitochondrial preparations – isolated mitochondria, tissue  
154 homogenates, permeabilized tissues and cells. MgG remains outside of the mitochondrial  
155 matrix and fluoresces when bound to Mg<sup>2+</sup>. In the phosphorylation reaction



157 reactants and MgG bind Mg<sup>2+</sup> according to their apparent dissociation constants. When  
158 ADP is added to the experimental chamber, there is a fast drop of the fluorescence signal.  
159 If mitochondria and fuel substrates are present, ATP is generated and exchanged with  
160 ADP by the ANT. ATP has a higher affinity to Mg<sup>2+</sup> compared to ADP. As ATP concentration  
161 increases in the medium, the free Mg<sup>2+</sup> concentration declines, less MgG is bound to Mg<sup>2+</sup>,  
162 and the fluorescence decreases. The ATP concentration in the medium is calculated  
163 according to Chinopoulos et al (2009; 2014), taking in account that: (1) the initial  
164 concentration of ATP is zero, (2) the initial concentration of ADP is known, (3) the  
165 concentration of Mg<sup>2+</sup> is measured, and (4) apparent *K<sub>d</sub>* values for ADP and ATP with Mg<sup>2+</sup>  
166 are obtained experimentally.  
167

168 The free  $Mg^{2+}$  concentration was calibrated in MiR05-MgG containing the  
169 mitochondrial sample, fuel substrates, carboxyatractyloside, and oligomycin.  $MgCl_2$  was  
170 titrated in 10 steps of 0.1 mM to obtain a non-linear fit for calibration of the amperometric  
171 signal. After calibration, the  $K_d$  of ADP and ATP for  $Mg^{2+}$  was determined for each  
172 experimental condition by performing multiple titrations with ADP or ATP.  
173

## 174 2.6. *Substrate-uncoupler-inhibitor-titration (SUIT) protocols*

175

176 Coupling control protocols (SUIT-006) assess different coupling control states -  
177 LEAK, OXPHOS and ET - at a constant electron-transfer-pathway state (Gnaiger et al  
178 2020). The effect of MgG on mitochondrial respiration was evaluated in its absence or  
179 presence (1.1  $\mu M$ ), which was added to the experimental chambers prior to sample  
180 addition. Since this fluorescent dye is diluted in water, and only a 2  $\mu L$  volume was added  
181 into the 2 mL chamber, no solvent addition was performed in the control group without  
182 MgG. After addition of isolated mitochondria into the O2k chambers, residual oxygen  
183 consumption  $Rox$  was measured in the absence of substrates. Two coupling-control  
184 protocols were used to study simultaneously oxygen consumption and ATP production  
185 with the following titrations: NADH-pathway with 5 mM pyruvate and 2 mM malate, or  
186 Succinate-pathway with 0.5  $\mu M$  rotenone and 10 mM succinate. First, LEAK respiration  
187 was measured in the absence of ADP. Secondly, OXPHOS capacity was measured after  
188 addition of 2 mM ADP. Oligomycin (7.5–10.0 nM) or carboxyatractyloside (0.3 – 0.4 mM)  
189 were added to induce again a LEAK state. This was followed by stepwise titration of the  
190 uncouplers CCCP (0.5  $\mu M$  steps) or SF 6847 (25–50 nM steps) up to the optimum  
191 concentration, when the maximum  $O_2$  flux was achieved as a measure of ET capacity.  
192 Finally, residual oxygen consumption was measured after the addition of the CIII inhibitor  
193 antimycin A (2.5  $\mu M$ ).  
194

## 195 2.7. *Data analysis*

196

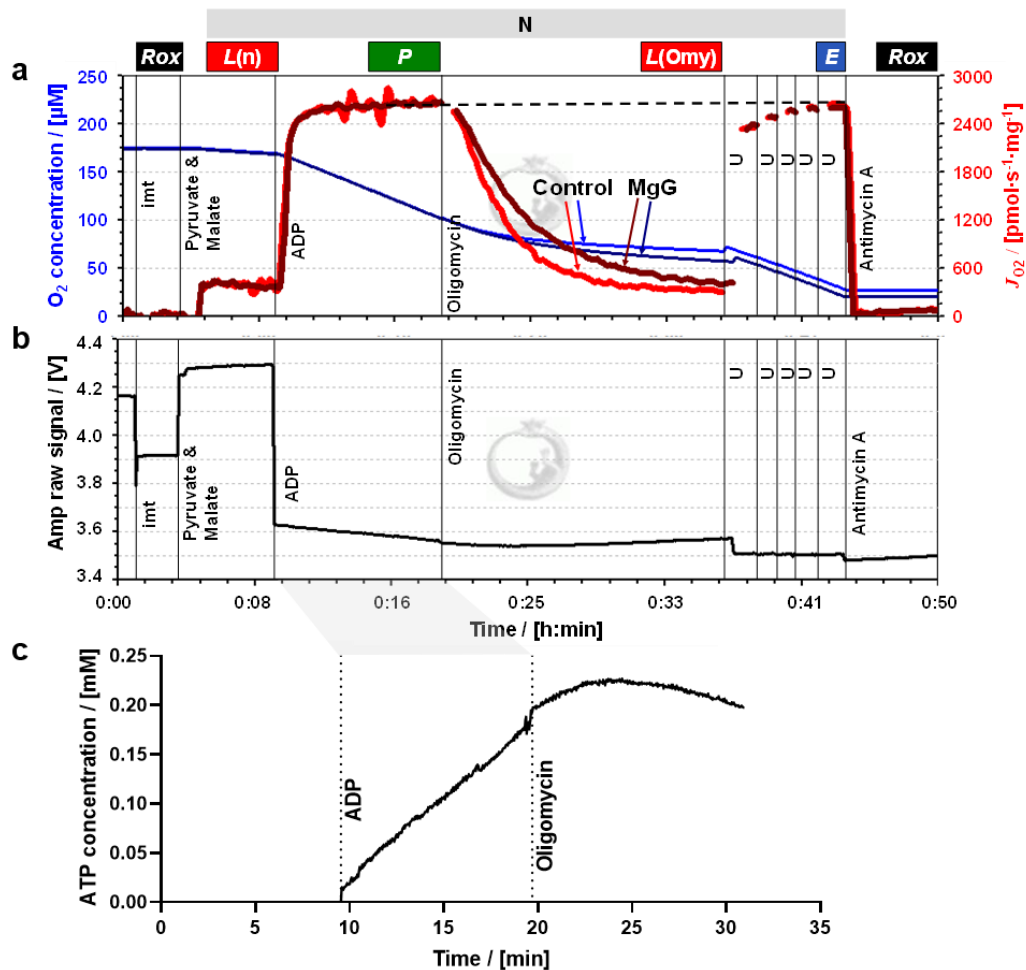
197 The assays were repeated 3 times with independent mitochondrial preparations,  
198 with or without MgG, for each condition tested. Data analysis for  $O_2$  consumption,  
199 calculations of  $K_d$  values and ATP production following Chinopoulos et al 2014, were  
200 performed using the templates provided with the software DatLab 7.4.  
201

## 202 3. Results and discussion

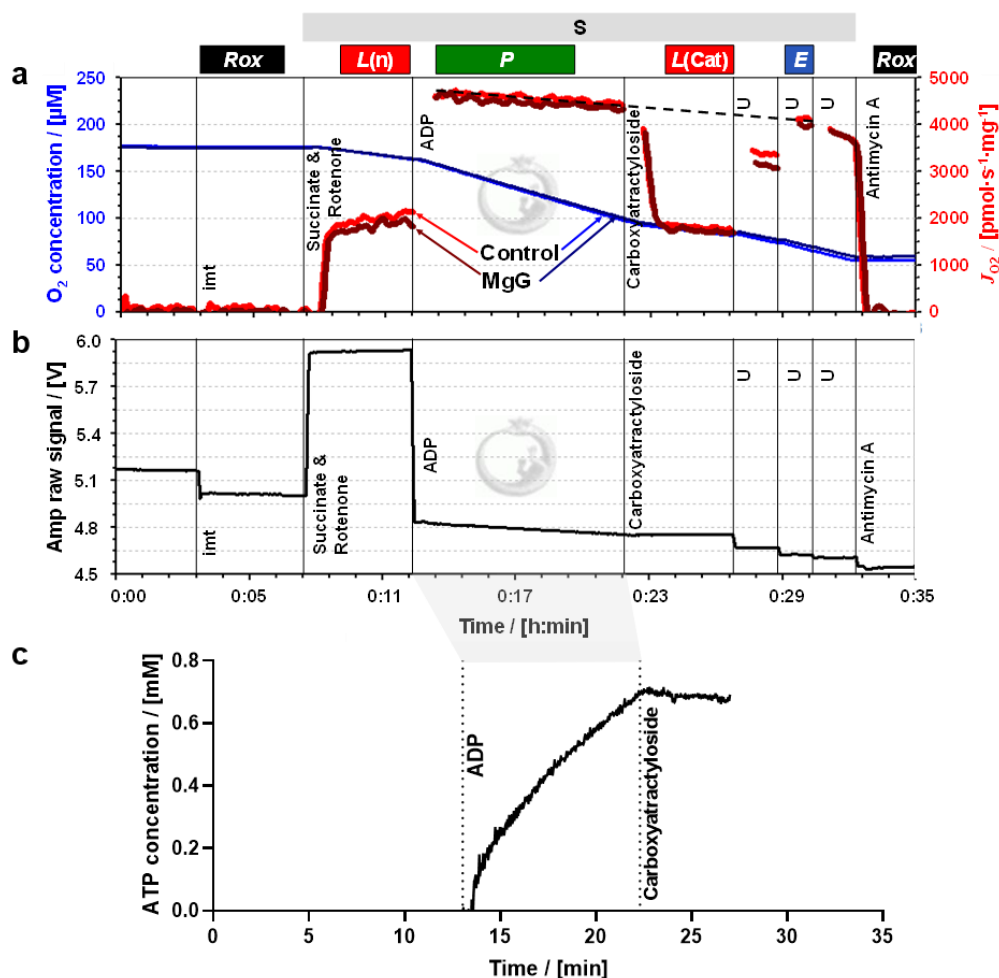
203

204 Figures 2a and 3a show superimposed traces of  $O_2$  concentration and  $O_2$  flux per  
205 mass. Coupling control of mitochondrial respiration was measured in two different  
206 electron-transfer-pathway control states. In the N-protocol, the NADH-linked pathway  
207 through Complex I (CI) was evaluated in the presence of pyruvate and malate which  
208 stimulate dehydrogenases of the TCA cycle, leading to reduction of  $NAD^+$  to NADH. NADH  
209 is the substrate of CI, with further electron flow into the Q-junction, CIII and CIV (Figure  
210 2). In the S-protocol, CI was inhibited by rotenone to prevent reverse electron transfer  
211 and accumulation of oxaloacetate, which is an inhibitor of succinate dehydrogenase  
212 (Makrecka-Kuka et al 2015; Gnaiger 2020), and respiration was measured supported by  
213 succinate as the substrate of CII (Figure 3).

214 In both protocols, LEAK respiration was measured (1)  $L(n)$ , in the absence of  
 215 adenylates and (2)  $L(Omy)$  or  $L(Cat)$ , in the presence of phosphorylation system  
 216 inhibitors. Respiration in these two LEAK states was similar, but slightly lower in  $L(Omy)$   
 217 with the N-protocol (Figure 2a, Table 1).  $L(n)$  stabilized quickly, whereas for  $L(Omy)$  it  
 218 took a long time to fully inhibit respiration by the low concentration of 7.5–10.0 nM  
 219 oligomycin. In the S-protocol with sequential addition of rotenone followed by succinate,  
 220  $L(n)$  increased for a few minutes until stabilization (Figure 3a). Inhibition by  
 221 carboxyatractyloside (0.3–0.4  $\mu\text{M}$ ) was immediate, and  $L(Cat)$  tended to be slightly lower  
 222 than  $L(n)$  (Table 1).  
 223



224 **Figure 2. Simultaneous measurement of respiration and ATP production by high-**  
 225 **resolution Fluorespirometry in mitochondria isolated from mouse heart.**  
 226 Representative traces for coupling control protocol SUIT-006 with NADH-linked  
 227 substrates (N-protocol), following additions (respiratory states): isolated mitochondria  
 228 imt (ROX), pyruvate & malate (LEAK), ADP (OXPHOS), oligomycin (LEAK), uncoupler U  
 229 (ET), and antimycin A (ROX). Experiment 2019-02-07 P5 04: **(a)**  $\text{O}_2$  concentration (dark  
 230 and lighter blue traces) and  $\text{O}_2$  flux per mass (dark and lighter red), 1.1  $\mu\text{M}$  MgG versus  
 231 control; **(b)** MgG fluorescence signal; **(c)** ATP concentration calculated from MgG signal  
 232 calibrated as  $\text{Mg}^{2+}$  concentration.  
 233



234  
 235 **Figure 3. Simultaneous measurement of respiration and ATP production by high-**  
 236 **resolution Fluorespirometry in mitochondria isolated from mouse heart.**  
 237 Representative traces for coupling control protocol SUIT-006 with succinate as substrate  
 238 (S-protocol), following additions (respiratory states): isolated mitochondria imt (ROX),  
 239 succinate & rotenone (LEAK), ADP (OXPHOS), carboxyatractyloside (LEAK), uncoupler U  
 240 (ET), and antimycin A (ROX). Experiment 2019-03-18 P5-03: (a)  $O_2$  concentration (dark  
 241 and lighter blue traces) and  $O_2$  flux per mass (dark and lighter red), 1.1  $\mu\text{M}$  MgG versus  
 242 control; (b) MgG fluorescence signal; (c) ATP concentration calculated from MgG signal  
 243 calibrated as  $\text{Mg}^{2+}$  concentration.

244  
 245 OXPHOS capacity  $P$  was measured in the presence of a kinetically saturating  
 246 concentration of ADP. The optimum uncoupler concentrations to measure maximum ET  
 247 capacity  $E$  were 6.0–7.0  $\mu\text{M}$  CCCP in the N-protocol, and 0.150–0.175  $\mu\text{M}$  SF 6847 in the  
 248 S-protocol. In the N-protocol,  $P$  was stable over time and identical to  $E$ . However, in the  
 249 S-protocol,  $P$  showed a slight decrease over time. Extrapolating this trend of declining  $O_2$   
 250 flux to the point where ET capacity was measured explains why  $E$  appears to be lower  
 251 than  $P$  (dashed trendline, Figure 3a). In both protocols, therefore,  $E = P$ , indicating that  
 252 OXPHOS capacity was not limited by the phosphorylation system. This agrees with results

253 for mouse heart mitochondria on coupling control even in the combined NS-pathway  
254 (Lemieux et al 2017). Parallel measurements were performed in the presence and  
255 absence of 1.1  $\mu\text{M}$  MgG with the N- and S-protocol. This low concentration of MgG used is  
256 sufficiently high for calculating ATP production (Figures 2b and c and Figures 3b and c).  
257

258 The MgG assay to measure ATP production can be used concomitantly with high-  
259 resolution respirometry, providing information real-time. Other methods are available to  
260 detect ATP production real-time. Spectrophotometric detection of NADPH can be used in  
261 conjunction with the coupled enzyme system hexokinase and glucose-6-phosphate  
262 dehydrogenase (Horgan, 1978). This assay has been adapted for simultaneous detection  
263 of  $\text{O}_2$  consumption and NADPH (Lark et al 2016). The luciferin/luciferase assay can be  
264 used for continuous measurement of ATP production (Manfredi et al 2002). It is  
265 important to note that luciferase consumes  $\text{O}_2$ , and instruments typically used for  
266 luminometry do not allow monitoring of  $\text{O}_2$  concentration in parallel.  
267

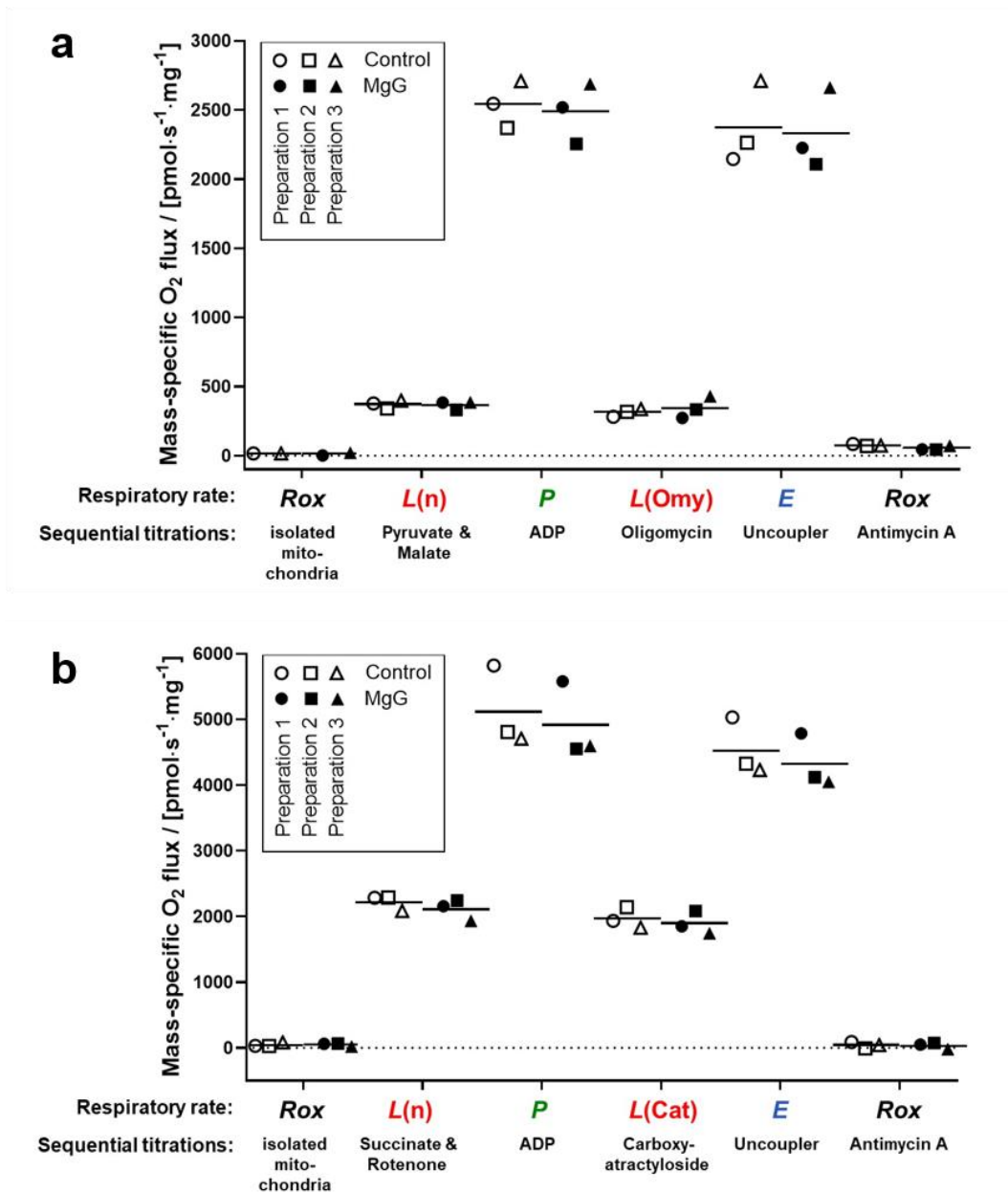
268 Another method for continuous measurement of the  $\text{P}\gg/\text{O}_2$  ratio is the steady-state  
269 ADP injection-respirometry (Gnaiger et al 2000b; 2001). The phosphorylation rate is set  
270 by continuous injection of ADP as the rate-limiting step while measuring  $\text{O}_2$  consumption  
271 stimulated to a constant sub-maximal level. Chance and Williams (1955) originally  
272 described a polarographic ADP pulse-titration method to determine the  $\text{P}\gg/\text{O}_2$  ratio,  
273 titrating a known concentration of ADP, which leads to a peak of  $\text{O}_2$  consumption  
274 stimulated by the complete phosphorylation of ADP to ATP. The ADP pulse-titration  
275 method has been extended and critically discussed by Gnaiger (2001).  
276

277 End-point assays are available to detect ATP levels, providing discontinuous  
278 measurement of ATP production. These include chromatography (high performance  
279 liquid chromatography, HPLC; thin layer chromatography, TLC); nuclear magnetic  
280 resonance detection of 2-deoxyglucose and its phosphorylated form, and radioactivity  
281 measurements using  $^{32}\text{P}$  (Menegollo et al 2019; Morciano et al 2017; Fink et al 2017;  
282 Sausen et al 2019).  
283

284 The fluorometric MgG assay applied simultaneously with  $\text{O}_2$  consumption by HRR  
285 has been used extensively (Iftikar, Hickey 2013; Goo et al 2013; Chinopoulos et al 2014;  
286 Pham et al 2014; Power et al 2014; Salin et al 2016; Napa et al 2017; Masson et al 2017;  
287 Salin et al 2018; Devaux et al 2019; Salin et al 2019). Understanding whether MgG may  
288 affect respiration is crucial for such studies, particularly for  $\text{P}\gg/\text{O}_2$  ratios obtained in  
289 different electron-transfer-pathway states.  
290

291 It is well established that different dyes commonly applied to measure  
292 mitochondrial membrane potential inhibit OXPHOS capacity, *e.g.*, safranin, rhodamine  
293 123 and its derivatives TMRM and TMRE (Krumshnabel et al 2014; Scaduto, Grotyohann  
294 1999). Surprisingly, Amplex UltraRed used to detect  $\text{H}_2\text{O}_2$  flux impairs respiration despite  
295 not accumulating in the mitochondria (Makrecka-Kuka et al 2015). Therefore, we studied  
296 the effect of MgG on respiration. MgG at 1.1  $\mu\text{M}$  did not affect NADH-linked nor succinate-  
297 linked respiration in any coupling control state (LEAK, OXPHOS and ET) measured in  
298 mitochondria isolated from mouse hearts (Figure 4). In addition, residual oxygen  
299 consumption was not affected by MgG.  
300





301  
 302 **Figure 4. O<sub>2</sub> consumption in the absence and presence of MgG by mitochondria**  
 303 **isolated from mouse heart.** The respiratory rates indicated in the abscissa were  
 304 measured by HRR with two coupling control protocols SUIT-006, with the following  
 305 respiratory states: ROX, LEAK (in the absence of adenylates), OXPHOS, LEAK (in the  
 306 presence of inhibitors), ET, and ROX. Sequential titrations are described for **(a)** N-  
 307 protocol (experiments 2019-02-05 P3-04, 2019-02-06 P3-03 and 2019-02-07 P5-04) and  
 308 **(b)** S-protocol (experiments 2019-03-13 P6-03, 2019-03-14 P3-03 and 2019-03-18 P5-  
 309 03). For both graphs the three symbol shapes show independent mitochondrial  
 310 preparations, whereas open and closed symbols compare results in controls and in the  
 311 presence of MgG from the same preparation; bars represent the average.  
 312

313 **Table 1. Coupling control efficiency  $(P-L)/P$  and  $P_{\gg}/O_2$  ratio in absence or presence**  
 314 **of MgG.** Average  $\pm$  SD,  $N=3$ . OXPHOS capacity  $P$  and LEAK respiration  $L$  corrected for  
 315 residual oxygen consumption  $Rox$ .  $L(n)/L(inh)$  ratios:  $L$  in the absence of adenylates ( $n$ )  
 316 over  $L$  with an inhibitor ( $inh$ ) of the phosphorylation system, oligomycin Omy or  
 317 carboxyatractyloside Cat for the N- or S-pathway, respectively.  $L(inh)$  is used in  $(P-L)/P$ .

Protocol	$(P-L)/P$	$L(n)/L(inh)$	$P_{\gg}/O_2$	$P_{\gg}/O$
N-pathway - MgG	$0.90 \pm 0.01$	$1.13 \pm 0.05$	-	-
N-pathway + MgG	$0.88 \pm 0.02$	$1.12 \pm 0.04$	$2.33 \pm 1.07$	$1.16 \pm 0.53$
S-pathway - MgG	$0.62 \pm 0.05$	$1.27 \pm 0.16$	-	-
S-pathway + MgG	$0.61 \pm 0.05$	$1.12 \pm 0.26$	$2.78 \pm 0.74$	$1.39 \pm 0.37$

318  
 319 The NADH-pathway has three coupling sites, CI, CIII and CIV, whereas the succinate-  
 320 pathway has only the latter two, resulting in a lower  $P_{\gg}/O_2$  ratio. When dividing ATP flux,  
 321 calculated from the increase in ATP concentration per time, by the simultaneously  
 322 measured  $O_2$  flux, then  $P_{\gg}/O_2$  flux ratios ( $J_{P_{\gg}}/J_{O_2}$ ) are obtained. The  $P_{\gg}/O_2$  is twice the  
 323 classical  $P_{\gg}/O$  (Table 1).  $P_{\gg}/O_2$  obtained for S-pathway was close to the theoretically  
 324 expected value (Gnaiger et al 2020). The result obtained for N-pathway was lower than  
 325 expected. A limitation of the present study is the low number of replicates ( $N = 3$ ), with a  
 326 high variability of  $P_{\gg}/O_2$  ratios. Further experiments are in preparation.

327  
 328 Coupling control efficiencies are closely related to  $P_{\gg}/O_2$  ratios. The coupling  
 329 control efficiency is defined as  $(E-L)/E$ , ranging from 0, at zero coupling, to 1 in a fully  
 330 coupled system. In the present case of  $P = E$ , the coupling control efficiency is expressed  
 331 as the  $P-L$  control efficiency,  $(P-L)/P$  (Gnaiger 2020). As expected, a higher  $P-L$  control  
 332 efficiency of  $0.89 \pm 0.02$  was found for the N-pathway than  $0.62 \pm 0.05$  for the S-pathway  
 333 (pooled data with and without MgG, average  $\pm$  standard deviation,  $N = 6$ ; Table 1). These  
 334 correspond to a RCR =  $P/L$  of  $9.6 \pm 1.8$  for the N-pathway and  $2.6 \pm 0.3$  for the S-pathway.

335  
 336 In summary, MgG did not affect respiration in any of the coupling control states.  
 337 These results demonstrate that measurement of  $O_2$  consumption is reliable concomitant  
 338 with the MgG assay in SUIT protocols with different pathway states and coupling states.  
 339

### 340 Acknowledgements

341 We thank Marco Di Marcello and Manuela Passrigger for expert technical support on media and  
 342 chemicals preparation, equipment maintenance and mitochondria isolation. This work was  
 343 partially funded by the European Union's Horizon 2020 research and innovation programme  
 344 under grant agreement No. 859770, NextGen-O2k project. Contribution to COST Action CA15203  
 345 MitoEAGLE.  
 346

### 347 Author contributions

348 LHDC, CD and EG designed the work; LHDC collected and analyzed data and drafted the article;  
 349 CD and EG critically revised the article, all authors approved the final version of the manuscript.  
 350

### 351 Conflicts of interest

352 EG is founder and CEO of Oroboros Instruments, Innsbruck, Austria.  
 353

### 354 Data availability

355 Original files are available Open Access at Zenodo repository: [10.5281/zenodo.4032674](https://doi.org/10.5281/zenodo.4032674).

## 356 Abbreviations

357 Amp amperometric; ANT adenosine nucleotide translocase; BSA bovine serum albumin; CI to CIV  
358 Complex I to IV; CCCP carbonyl cyanide m-chlorophenyl hydrazone;  $\Delta\Psi_p+$  mt-membrane  
359 potential; EGTA ethylene glycol tetraacetic acid; *E* ET capacity; ETS electron transfer system;  $F_0F_1$   
360 ATP synthase; Hepes *N*-(2-hydroxyethyl)piperazine-*N'*-(2-ethanesulfonic acid); HRR high-  
361 resolution respirometry; imt isolated mitochondria;  $J_{O_2}$   $O_2$  flux;  $K_d$  dissociation constant; *L* LEAK  
362 respiration; LED light-emitting diode; MES 2-(*N*-morpholino)ethanesulfonic acid hydrate; MgG  
363 Magnesium Green; *P* OXPHOS capacity;  $P_{\gg}/O$  ADP phosphorylated per atom oxygen consumed;  
364  $P_{\gg}/O_2$  ADP phosphorylated per molecular oxygen consumed;  $P_i$  inorganic phosphate; RCR  
365 respiratory acceptor control ratio; *Rox* residual oxygen consumption; SUIT substrate-uncoupler -  
366 inhibitor-titration; TCA tricarboxylic acid; TMRM tetramethylrhodamine methyl ester; TMRE  
367 tetramethylrhodamine ethyl ester;  $TPP^+$  tetraphenylphosphonium; Tris 2-amino-2-  
368 (hydroxymethyl)-1,3-propanediol; U uncoupler.

## 370 References

- 371  
372 Budinger GRS, Duranteau J, Chandel NS, Schumacker PT (1998) Hibernation during hypoxia in  
373 cardiomyocytes. Role of mitochondria as the  $O_2$  sensor. *J Biol Chem* 273:3320-6.  
374 Chance B, Williams GR (1955) Respiratory enzymes in oxidative phosphorylation. I. Kinetics of oxygen  
375 utilization. *J Biol Chem* 217:383-93.  
376 Chinopoulos C, Vajda S, Csanady L, Mandi M, Mathe K, Adam-Vizi V (2009) A Novel Kinetic Assay of  
377 Mitochondrial ATP-ADP Exchange Rate Mediated by the ANT. *Biophys J* 96:2490-504.  
378 Chinopoulos C, Kiss G, Kawamata H, Starkov AA (2014) Measurement of ADP-ATP exchange in relation to  
379 mitochondrial transmembrane potential and oxygen consumption. *Methods Enzymol* 542:333-48.  
380 Devaux JBL, Hedges CP, Birch N, Herbert N, Renshaw GMC, Hickey AJR (2019) Acidosis maintains the  
381 function of brain mitochondria in hypoxia-tolerant triplefin fish: a strategy to survive acute hypoxic  
382 exposure? *Front Physiol* 9:1941.  
383 Doerrier C, Garcia-Souza LF, Krumschnabel G, Wohlfarter Y, Mészáros AT, Gnaiger E (2018) High-  
384 Resolution FluoRespirometry and OXPHOS protocols for human cells, permeabilized fibers from small  
385 biopsies of muscle, and isolated mitochondria. *Methods Mol Biol* 1782:31-70.  
386 Fink BD, Bai F, Yu L, Sivitz WI (2017) Regulation of ATP production: dependence on calcium concentration  
387 and respiratory state. *Am J Physiol Cell Physiol* 313:C146-53.  
388 Fontana M, Krumschnabel G (2015) Isolation of mouse heart mitochondria. *Mitochondr Physiol Network*  
389 20.06(01):1-2.  
390 Fontana-Ayoub M, Fasching M, Gnaiger E (2016) Selected media and chemicals for respirometry with  
391 mitochondrial preparations. *Mitochondr Physiol Network* 03.02(18):1-10.  
392 Gnaiger E, Wyss M (1994) Chemical forces in the cell: Calculation for the ATP system. In: *What is Controlling*  
393 *Life?* (Gnaiger E, Gellerich FN, Wyss M, eds) *Modern Trends in BioThermoKinetics* 3. Innsbruck Univ  
394 Press:207-12.  
395 Gnaiger E (2001) Bioenergetics at low oxygen: dependence of respiration and phosphorylation on oxygen  
396 and adenosine diphosphate supply. *Respir Physiol* 128:277-97.  
397 Gnaiger E (2020) Mitochondrial pathways and respiratory control. An introduction to OXPHOS analysis. 5th  
398 ed. *Bioenerg Commun* 2020.2: 112 pp. doi:10.26124/bec:2020-0002.  
399 Gnaiger E et al – MitoEAGLE Task Group (2020) Mitochondrial physiology. *Bioenerg Commun* 2020.1.  
400 doi:10.26124/bec:2020-0001.v1.  
401 Gnaiger E, Kuznetsov AV, Schneeberger S, Seiler R, Brandacher G, Steurer W, Margreiter R (2000a)  
402 Mitochondria in the cold. In: *Life in the Cold* (Heldmaier G, Klingenspor M, eds) Springer, Heidelberg,  
403 Berlin, New York:431-42.  
404 Gnaiger E, Méndez G, Hand SC (2000b) High phosphorylation efficiency and depression of uncoupled  
405 respiration in mitochondria under hypoxia. *Proc Natl Acad Sci U S A* 97:11080-5.  
406 Goo S, Pham T, Han JC, Nielsen P, Taberner A, Hickey A, Loiselle D (2013) Multiscale measurement of cardiac  
407 energetics. *Clin Exp Pharmacol Physiol* 40:671-81.

- 408 Horgan DJ (1978) A spectrophotometric assay of ATP synthesized by sarcoplasmic reticulum. *Aust J Biol Sci*  
 409 31:21-4.
- 410 Iftikar FI, Hickey AJ (2013) Do mitochondria limit hot fish hearts? Understanding the role of mitochondrial  
 411 function with heat stress in *Notolabrus celidotus*. *PLoS One* 8:e64120.
- 412 Krumschnabel G, Eigentler A, Fasching M, Gnaiger E (2014) Use of safranin for the assessment of  
 413 mitochondrial membrane potential by high-resolution respirometry and fluorometry. *Methods Enzymol*  
 414 542:163-81.
- 415 Lark DS, Torres MJ, Lin CT, Ryan TE, Anderson EJ, Neuffer PD (2016) Direct real-time quantification of  
 416 mitochondrial oxidative phosphorylation efficiency in permeabilized skeletal muscle myofibers. *Am J*  
 417 *Physiol Cell Physiol* 311:C239-45.
- 418 Lemieux H, Blier PU, Gnaiger E (2017) Remodeling pathway control of mitochondrial respiratory capacity  
 419 by temperature in mouse heart: electron flow through the Q-junction in permeabilized fibers. *Sci Rep*  
 420 7:2840, DOI:10.1038/s41598-017-02789-8.
- 421 Leysens A, Nowicky AV, Patterson L, Crompton M, Duchon MR (1996) The relationship between  
 422 mitochondrial state, ATP hydrolysis,  $[Mg^{2+}]_i$  and  $[Ca^{2+}]_i$  studied in isolated rat cardiomyocytes. *J Physiol*  
 423 496:111-28.
- 424 Lowry OH, Rosebrough NJ, Farr AL, Randall RJ (1951) Protein measurement with the Folin phenol reagent.  
 425 *J Biol Chem* 193:265-275.
- 426 Makrecka-Kuka M, Krumschnabel G, Gnaiger E (2015) High-resolution respirometry for simultaneous  
 427 measurement of oxygen and hydrogen peroxide fluxes in permeabilized cells, tissue homogenate and  
 428 isolated mitochondria. *Biomolecules* 5:1319-38.
- 429 Manfredi G, Yang L, Gajewski CD, Mattiazzi M (2002) Measurements of ATP in mammalian cells. *Methods*  
 430 26:317-26.
- 431 Masson SWC, Hedges CP, Devaux JBL, James CS, Hickey AJR (2017) Mitochondrial glycerol 3-phosphate  
 432 facilitates bumblebee pre-flight thermogenesis. *Sci Rep* 7:13107.
- 433 Menegollo M, Tessari I, Bubacco L, Szabadkai G (2019) Determination of ATP, ADP, and AMP Levels by  
 434 Reversed-Phase High-Performance Liquid Chromatography in Cultured Cells. *Methods Mol Biol*  
 435 1925:223-32.
- 436 Morciano G, Sarti AC, Marchi S, Missiroli S, Falzoni S, Raffaghello L, Pistoia V, Giorgi C, Di Virgilio F, Pinton P  
 437 (2017) Use of luciferase probes to measure ATP in living cells and animals. *Nat Protoc* 12:1542-62.
- 438 Napa K, Baeder AC, Witt JE, Rayburn ST, Miller MG, Dallon BW, Gibbs JL, Wilcox SH, Winden DR, Smith JH,  
 439 Reynolds PR, Bikman BT (2017) LPS from *P. gingivalis* negatively alters gingival cell mitochondrial  
 440 bioenergetics. *Int J Dent* 2017:2697210.
- 441 Pham T, Loisel D, Power A, Hickey AJ (2014) Mitochondrial inefficiencies and anoxic ATP hydrolysis  
 442 capacities in diabetic rat heart. *Am J Physiol* 307:C499-507.
- 443 Power A, Pearson N, Pham T, Cheung C, Phillips A, Hickey A (2014) Uncoupling of oxidative phosphorylation  
 444 and ATP synthase reversal within the hyperthermic heart. *Physiol Rep* pii:e12138.
- 445 Salin K, Villasevil EM, Auer SK, Anderson GJ, Selman C, Metcalfe NB, Chinopoulos C (2016) Simultaneous  
 446 measurement of mitochondrial respiration and ATP production in tissue homogenates and calculation  
 447 of effective P/O ratios. *Physiol Rep* 10.14814/phy2.13007.
- 448 Salin K, Villasevil EM, Anderson GJ, Selman C, Chinopoulos C, Metcalfe NB (2018) The RCR and ATP/O  
 449 indices can give contradictory messages about mitochondrial efficiency. *Integr Comp Biol* 58:486-94.
- 450 Salin K, Villasevil EM, Anderson GJ, Lamarre SG, Melanson CA, McCarthy I, Selman C, Metcalfe NB (2019)  
 451 Differences in mitochondrial efficiency explain individual variation in growth performance. *Proc Biol Sci*  
 452 286:20191466.
- 453 Sausen CW, Rogers CM, Bochman ML (2019) Thin-Layer Chromatography and Real-Time Coupled Assays  
 454 to Measure ATP Hydrolysis. *Methods Mol Biol* 1999:245-253.
- 455 Scaduto RC Jr, Grotyohann LW (1999) Measurement of mitochondrial membrane potential using  
 456 fluorescent rhodamine derivatives. *Biophys J* 76:469-77.

457  
 458 **Copyright:** © 2021 The authors. This is an Open Access preprint (not peer-reviewed) distributed  
 459 under the terms of the Creative Commons Attribution License, which permits unrestricted use,  
 460 distribution, and reproduction in any medium, provided the original authors and source are  
 461 credited. © remains with the authors, who have granted MitoFit Preprints an Open Access  
 462 publication license in perpetuity.

